Two-photon induced exciton mediated dissociation of N_2O and photomobility of O atoms in crystalline Xe

W. G. Lawrence and V. A. Apkarian[a)]
Department of Chemistry, University of California, Irvine, California 92717

(Received 7 May 1992; accepted 24 July 1992)

Two-photon induced access of Xe excitons at 248 nm leads to efficient dissociation of N_2O impurities via ionic potentials. The product O atoms are probed via the Xe^+O^- charge transfer transitions, and the N_2O disappearance is probed by infrared (IR) spectroscopy. Charge transfer excitation of O atoms leads to atomic mobility, such that with extensive irradiation a photochemical steady-state is reached between N_2O, oxygen atoms trapped in the Xe bulk, and within the same cage as N_2. A detailed kinetic analysis of these processes is presented. Among the extracted parameters are the two-photon absorption cross section of Xe at 248 nm, 3.7×10^{-48} cm^4 s, the free exciton migration length, 47 Å, and the excitonic dissociation probability of N_2O, 0.85. The mobility of photoexcited O atoms is attributed to the topology of electronically excited surfaces which show minima at the ground state cage barriers.

I. INTRODUCTION

Photodissociation studies of molecules trapped in rare gas solids often involve intense ultraviolet laser irradiation of highly diluted samples. Under such conditions, the primary irradiation energy may be predominantly deposited in the host lattice via multiphoton processes. Two-photon access of excitonic bands becomes possible for photon energies >4 eV in Xe, and 5 eV in Kr, the cross sections of which have recently been reported.[1] Given the large mobilities of free excitons, exciton-impurity encounters are highly probable.[2,3] Dissociation of molecular impurities is a possible outcome of an exciton–molecule encounter. We present experimental data from studies of N_2O photodissociation in solid xenon which reveal this mechanism, namely, two-photon induced access of excitonic states and subsequent molecular dissociation due to exciton–molecule encounters.

In the experimental studies to be described, the dissociation of N_2O is followed by monitoring the photogenerated O atoms, and by following the disappearance of N_2O. The first is accomplished by laser-induced fluorescence from the XeO charge transfer states, the spectroscopy of which was recently reported.[4] The second is achieved by monitoring N_2O by infrared absorption spectroscopy, details of which were also reported.[5] While oxygen atoms in their ground, ^3P, state are permanently trapped,[6] excitation to the charge transfer states can lead to mobility. In effect, both O^- and $O(^1D)$ have smaller interaction ranges with the lattice, and the kinetic energy acquired, due to differences in potential gradients in the ground and excited states, is sufficient to give the atoms mobility. Due to the facile migration of photoexcited O atoms, a photochemical steady state is observed between the two-photon dissociation of N_2O and one-photon induced recombination of O atoms. A detailed kinetic analysis of these photoprocesses is presented, and the dynamics is rationalized by the topography of electronic surfaces.

II. EXPERIMENT

The studies were carried out in 1 cm^3 free standing, polycrystalline solids. The details of sample preparation have been presented.[5] Premixed gas samples of N_2O/Xe ($\sim$1/10 000) were rapidly deposited onto a cryotip through an insulating mold to form the free standing crystals. An oil diffusion pump with a liquid nitrogen trap was used to maintain vacuum in the cryostat shroud and sample manifold. Xenon of 99.999% purity (Cryogenic Rare Gases), and N_2O of 99.9% purity (Matheson) were used, without further purification. Samples were mixed and stored in 5 *l* darkened glass bulbs. The large volume of the bulb prevented large changes in back pressure during crystal growth.

N_2O was dissociated and the oxygen atoms were detected using the same laser source. The majority of the experiments to be reported were carried out at 248 nm. Typically, intensities of <10 mJ/cm^2 in 20 ns pulses were used without focusing. Fluorescence was collected at right angles. Spectra were recorded using a $\frac{1}{4}$ m polychromator and an optical multichannel analyzer (EG&G OMA) equipped with a gated intensified diode array, with 950 active elements. The detection efficiency of the OMA was calibrated using a standard irradiance lamp with an effective black body temperature of 3100 K (Oriel model 63358). The wavelength calibration of the OMA is made using a Hg/argon pen-lamp. Laser scatter was blocked using a 1 cm path length liquid cell containing toluene, CCl_4, or methanol.

Infrared absorptions were used to monitor the N_2O concentration as a function of irradiation time. The dissociation laser was directed into the cryostat to overlap the infrared (IR) probe. The dissociation laser sources used were either the fourth harmonic of a Nd:YAG laser (Quanta Ray DCR2), or the 248 or 193 nm output of a multigas excimer laser (Lambda Physik EMG 53). To follow the dissociation of N_2O by its IR absorption, CaF_2 windows were used to transmit both the ultraviolet (UV) and IR beams. This limited the spectral range in the IR to

[a)]Alfred P. Sloan Fellow.

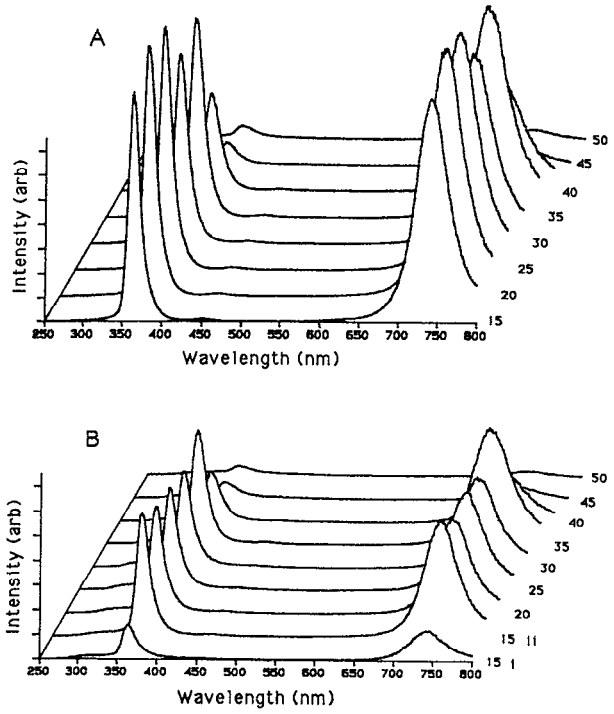

FIG. 1. Temperature dependent emission spectra of Xe^+O^- after dissociation of N_2O at 248 nm. (a) After the initial dissociation of N_2O in crystalline xenon shown as the first growth curve in Fig. 5. The concentration of oxygen atoms isolated in xenon is probed by 20 pulses at each temperature. Between 35 and 40 K the emission intensity begins to decrease. (b) The first emission spectrum of the series, labeled 15 i, is the spectrum recorded upon cooling the sample from 50 K (in a) to 15 K. The subsequent spectra are recorded after irradiation and regeneration of the Xe^+O^- emission shown by the second growth curve in Fig. 5.

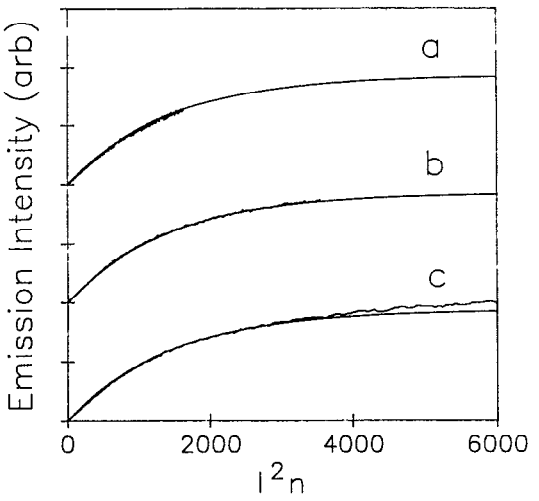

FIG. 2. Growth of Xe^+O^- emission upon irradiation of an N_2O/xenon crystalline sample vs I^2n, I=laser intensity, n=number of deposited laser pulses, at three different intensities (a) 4.2 mJ/cm^2; (b) 8.8 mJ/cm^2; (c) 16.8 mJ/cm^2. The three growth curves are fit to the same exponential which is shown for each curve.

frequencies $>1000\ cm^{-1}$, eliminating the possibility of observing the N_2O bending mode.

III. RESULTS

Oxygen atoms in solid Xe can be detected by their charge transfer emissions centered at 375 and 750 nm. In the case of interstitially trapped O atoms, the charge transfer bands can be reached by excitation in the wavelength range of 220–260 nm.[4] A sequence of emission spectra, obtained by 248 nm irradiation of the solid, is collected in Fig. 1. The first trace in Fig. 1(a) is obtained after extensive irradiation of the solid at 15 K. The sample is subsequently heated. The emissions subside between 40 and 50 K, but do not disappear completely. Upon cooling of the solid back to 15 K [first trace in Fig. 1(b)] only 10% of the initial intensity is retrieved. Subsequent irradiation of the solid at 15 K [second trace in Fig. 1(b)] regenerates the emission, and the entire process can be repeated. Thus, the photodissociation of N_2O to yield $O+N_2$ can be followed by monitoring the growth of these characteristic emissions as a function of irradiation time. Growth curves of XeO, when N_2O doped solid Xe of $M/R=10\,000$ are irradiated at 248 nm, are shown in Fig. 2. The initial growth rates show a square dependence on photon flux. This is illustrated in Fig. 2 by showing growth curves at different powers, which when plotted as a function of the square of irradiation intensity, yield identical exponential growth rates. In all cases, the initial exponential growth is followed by a linear slope, a pseudozero order rate of growth. From the exponential fits to the early part of the growth curves, $[O]=[O]_\infty\{1-\exp[-\sigma^{(2)}\phi I^2 t]\}$, an effective two-photon dissociation cross section, $\sigma^{(2)}\phi=5.8\times10^{-44}$ cm^4 s is obtained [in which $\sigma^{(2)}$ is a two-photon absorption cross section, and ϕ is a dissociation quantum yield]. The residual growth is indicative of the fact that the dissociation is not complete. This is verified by following infrared absorptions of N_2O.

In Fig. 3, the decay in IR absorptions of N_2O when the samples are irradiated at 266, 248, and 193 nm, are shown. Only a fraction of the N_2O is dissociated at 266 and 248 nm, 40% and 10%, respectively. The dissociation can be carried out to completion at 193 nm. We note the abscissa in these plots are extended by a factor of 10 beyond that of Fig. 1. The origin of the noise in the data are not well understood. The absorption cross sections of the stretching fundamentals in N_2O/Xe show an anomalous temperature dependence.[5] That absorption intensities are sensitive to the geometry of the immediate trap cage is to be expected, however not quantified. The determination of the exact fraction of undissociated molecules is subject to uncertainty due to possible mismatches between the UV irradiation volume, and the IR probe volume. This consideration is particularly severe in the case of the 266 nm measurements, since the UV beam has the characteristic doughnut mode profile of the tripled YAG laser used. As such the 40% dissociation limit reached in the case of the 266 nm irradiation should be regarded as an underestimate. It is, however, clear that at 193 nm, where N_2O has a strong absorption, one-photon dissociation of the molecule can be carried to completion, a process well characterized recently

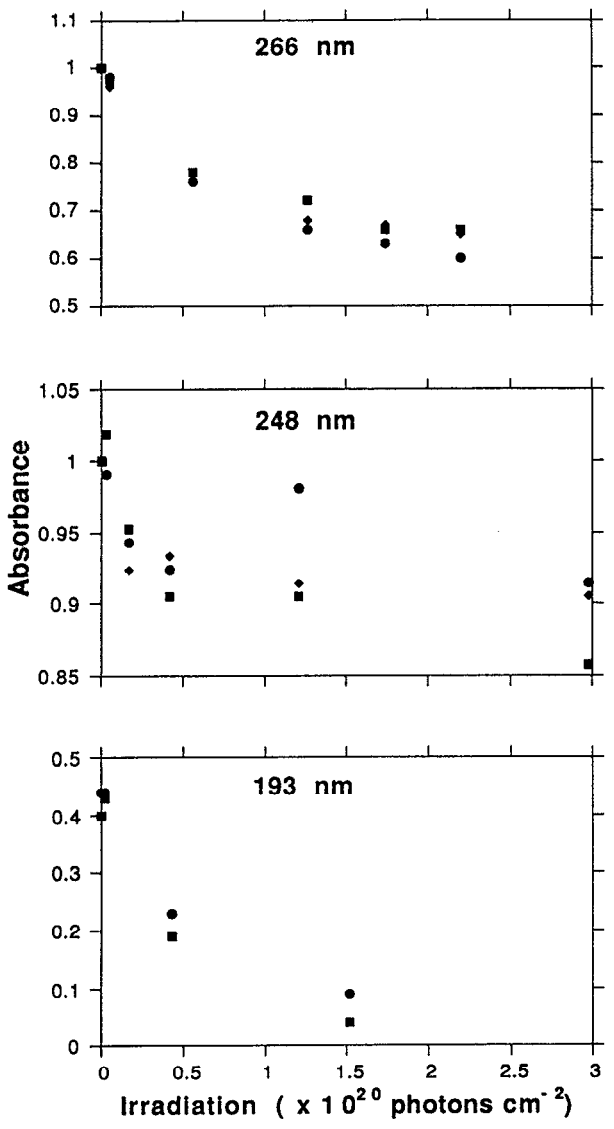

FIG. 3. Decrease of N_2O IR absorption intensity upon irradiation at 266, 248, and 193 nm measured by the 200 (●), 120 (■), and 100 (◆) absorption bands of N_2O. The dissociation pump powers used are $I_{266}=1.5\times10^{16}$ photons cm^{-2}, $I_{248}=1.3\times10^{16}$ photons cm^{-2}, and $I_{193}=5\times10^{15}$ photons cm^{-2}.

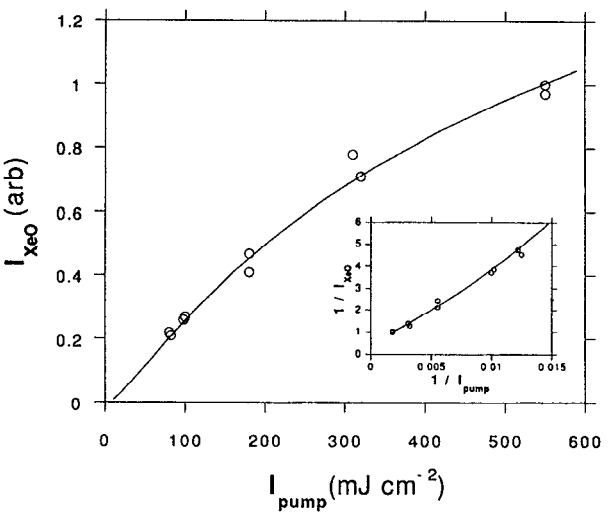

FIG. 4. Emission intensity of Xe^+O^- at the power dependent steady state concentration. The fit to the data using the parameters from the kinetic model at equilibrium is also shown (see text for details). The insert follows the notation used in Eq. (11) of the text, the slope of the fit yields the ratio $[N_2O]_e/[O/Xe]_e$, and the intercept yields the $[O/N_2]_e/[O/Xe]_e$ ratio.

in Xe matrices.[6] N_2O does not have significant absorptions either at 248 nm or at 266 nm. In both cases the dissociation proceeds via a two-photon mechanism. Note however that while 248 nm is strongly absorbed by O/Xe, 266 nm, which corresponds to the threshold of this absorption, is only weakly absorbed.[4]

It is possible to show that with extended 248 nm irradiation a photochemical steady-state is established in the O/Xe concentration. This is established by monitoring the plateau reached in the 750 nm emission. When the photogeneration is carried out at low power and then switched to high power the 750 nm emission grows to a new level. When the plateau is reached at high power, and then switched to low power, the emission intensity decays to a new lower limit. The O atom disappearance is therefore photo-induced. The dependence of the steady-state O atom concentration on pump intensity is illustrated in Fig. 4. The data in this case are collected by imaging the profile of the entire laser irradiated volume on the OMA (laser beam parallel to slit of polychromator). At each intensity, the sample is irradiated for a sufficiently long period to ensure that the emission intensity has reached a plateau. The same results are obtained whether the measurements are conducted as a function of increasing or decreasing laser intensity. Since the process can be reversed by changing laser intensity, it is necessary to conclude that photomobility leads to a sink from which the atoms can be regenerated by irradiation. The possible sinks of O atoms are formation of O_2, and retrapping of $O(^3P)$ next to N_2 (henceforth designated as O/N_2). For the latter to act as a sink, it is also necessary to assume that O atoms trapped in such sites are either inaccessible or that they do not emit, i.e., charge transfer states of XeO are quenched by N_2 (reactively or otherwise). To test the possibility of O_2 as the sink of O atoms, studies were carried out in O_2 doped Xe. Excitation of such solids at 248 nm does not lead to production of O atoms. We can therefore safely assume that a photochemical steady-state is reached between N_2O, O/N_2, and O/Xe.

In summary, at 248 nm, the early generation of O/Xe from N_2O is two-photon induced. After extensive irradiation, an intensity dependent photochemical steady-state is reached in the isolated O atom concentration. The overall process can therefore be presented by a cyclic kinetic scheme,

$$\begin{array}{ccc} N_2O+Xe+2h\nu & \rightleftarrows & O/Xe+h\nu \\ & \searrow\nwarrow \quad \nearrow\swarrow & \\ & O/N_2+h\nu & \end{array}$$

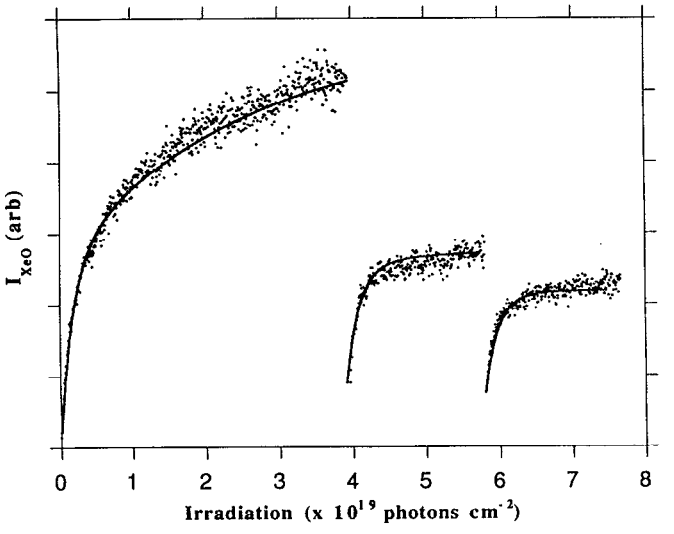

FIG. 5. Initial growth of Xe^+O^- emission intensity upon irradiation of an N_2O/xenon sample at 248 nm and the regeneration of the Xe^+O^- emission in the same sample after thermal cycles of 15 K→50 K→15 K. The initial growth and two regeneration cycles are shown together with the fit from the kinetic model presented in the text.

Thermal cycling experiments reinforce the above picture. After extensive irradiation, when the solids are warmed up, the O atom emissions subside. This was illustrated in Fig. 1. At 50 K, nearly 90% of the emission intensity is permanently lost, as established by monitoring the emission after cool-down (the loss is not due to a reduced quantum efficiency of fluorescence). Upon subsequent irradiation, it is possible to regenerate the emission. The new limit reached is usually lower than that prior to heating. This process can be repeated several times with similar results. The time profiles of emission growth for a typical set of three thermal cycles is illustrated in Fig. 5. We note that the growth rates after the thermal cycle are faster than the initial photogeneration rates. These observations indicate that thermally activated diffusion of O atoms leads to a sink, from which they can be regenerated very efficiently. As in the above discussion, O_2 can be eliminated as the sink. That the thermal diffusion does not lead directly to the formation of N_2O is verified by IR spectroscopy. We are forced to conclude that the sink is O/N_2, and that O atoms at such sites can be reached at 248 nm, but do not fluoresce. The fast rate of growth after heating the solid can then be attributed to the photoconversion of O/N_2 to O/Xe. Presumably, the energy released to the lattice, by quenching the XeO emission, can be used for cage exit of the O atoms.

From the thermal cycles we conclude that thermally induced mobility of O atoms leads to trapping of $O(^3P)$ atoms next to N_2, and that such atoms can be optically detrapped into the Xe bulk.

IV. DISCUSSION

The absorption of N_2O at 248 nm, which has been assigned to the forbidden $^1\Sigma^- \leftarrow {}^1\Sigma^+$ transition, is very weak, $\sigma^{(1)} \cong 10^{-24}$ cm^2.[7,8] The two-photon excitation cross section of Xe at the same wavelength has been measured in solid Xe to be $\sigma^{(2)} = 3.7 \times 10^{-48}$ cm^4 s. For an optically thin sample, the competition between one-photon excitation of an impurity vs the two-photon excitation of the host can be estimated as

$$(\Delta I/I)^{(1)}/(\Delta I/I)^{(2)} \sim \sigma^{(1)}/[I\sigma^{(2)}M/R].$$

At a typical photon flux of $I = 1.5 \times 10^{23}$ photons cm^{-2} s^{-1} (1 mJ cm^{-2}, 10 ns pulse width, 5 eV photons) and at a dilution of $M/R = 10\,000$, the above ratio yields 10^{-4}, i.e., the radiation is primarily deposited in the Xe host. The two-photon absorption cross section of N_2O at 248 nm has been reported as 3×10^{-51} cm^4 s.[9] Therefore, unless a dramatic enhancement of this cross section (of seven orders of magnitude) occurs, its effect would be negligible in comparison to that of the Xe host.

From the initial rate of growth of O atoms (see Fig. 2), a two-photon photogeneration rate of 5.8×10^{-44} cm^4 s is obtained. If we take the dilution factor of N_2O of 10^4 into account, this rate would, within the experimental errors of measurement, correspond to $\sigma^{(2)}$, the two-photon absorption cross section of Xe. Since the measured rate is one of photogeneration, its agreement with the absorption cross section would imply that dissociative trapping of the excitons at the N_2O sites proceeds with nearly unit probability. With extended irradiation, absorption by the photogenerated O atoms becomes significant. The charge transfer absorption of O/Xe is centered at 240 nm, with a full-width at half-maximum (FWHM) of 20 nm, and a radiative lifetime of 227 ns.[4] It is therefore possible to estimate an absorption cross section of 1×10^{-18} cm^2 at 248 nm. If it were possible to carry the dissociation of N_2O to completion, quite clearly absorption by O/Xe would dominate all photoprocesses. Given the 1 cm length of these solids, the assumption that the sample is optically thin throughout the irradiation period breaks down. With these considerations in mind, it becomes clear that a full account of the various photoprocesses requires a detailed kinetic analysis, for which we resort to numerical methods.

A. Kinetic model

The photogeneration step is described by the kinetic equations

$$\begin{aligned}
&Xe + 2h\nu && \rightarrow Xe^{**} && ;\sigma^{(2)}, && (1)\\
&Xe^{**} + N_2O && \rightarrow N_2O && ;k_2\phi_{21}, && (2a)\\
& && \rightarrow O/N_2 && ;k_2\phi_{22}, && (2b)\\
& && \rightarrow N_2 + O/Xe && ;k_2\phi_{23}, && (2c)\\
&Xe^{**} && \rightarrow Xe^{*} && ;k_3, && (3)
\end{aligned}$$

in which Xe** represents a free exciton, while Xe* represents a self-trapped exciton; k_3 represents the rate constant for self-trapping, and self-trapped excitons are assumed to decay without further dynamics of relevance. The exciton encounter with N_2O is characterized by the bimolecular rate constant k_2 in Eqs. (2). The important model parameter with respect to the excitonic dynamics is k_2/k_3, which

represents the volume spanned by the free exciton prior to self-trapping. Upon trapping at an N_2O site, three possible outcomes are anticipated, quenching of the exciton by energy transfer to N_2O (2a), dissociation of N_2O without cage exit of fragments (2b), and dissociation by cage exit of the O atoms (2c). Note that $\phi_{21}+\phi_{22}+\phi_{23}=1$.

The photomobility of O atoms excited at 248 nm is represented by

$$\begin{aligned} O/Xe+h\nu \rightarrow Xe^+O^- &\rightarrow O/Xe+h\nu' &;\sigma_1\phi_{41}, &\quad (4a)\\ &\rightarrow O/N_2 &;\sigma_1\phi_{42}, &\quad (4b)\\ &\rightarrow N_2O &;\sigma_1\phi_{43}, &\quad (4c)\end{aligned}$$

in which it is assumed that the charge transfer absorption of O atoms trapped in the Xe bulk, with an absorption cross section of σ_1, proceeds via three possible outcomes, radiative relaxation with no further dynamics (4a), photomobility leading to re-entry of the initial cage (4b), and photomobility leading to recombination with N_2 (4c). The process of Eq. (4b) would be consistent with cage reentry of an O atom on the ^3P surface, while Eq. (4c) would be consistent with re-entry either as O^- or $O(^1D)$.

The above kinetic equations cannot account for the thermal cycling experiments in which a faster rate of O atom growth is observed after heating the solids. Thermal loss of O atoms necessarily proceeds on the ^3P surface, and will therefore lead to formation of O/N_2. Explicit account of regeneration of O/Xe from such sites is necessary

$$\begin{aligned} O/N_2+h\nu \rightarrow Xe^+O^- &\rightarrow O/N_2 &;\sigma_2\phi_{51}, &\quad (5a)\\ &\rightarrow O/Xe &;\sigma_2\phi_{52}, &\quad (5b)\\ &\rightarrow N_2O &;\sigma_2\phi_{53}. &\quad (5c)\end{aligned}$$

In Eq. (5), the charge transfer absorption of O atoms trapped in the same cage as N_2 is considered with the three possible outcomes of quenching without further dynamics 5(a), cage exit (5b), and recombination within the cage (5c). Note the absorption cross section in Eq. (5) need not be the same as the absorption cross section in Eq. (4).

Given the short lifetime of free excitons, ~ 1 ps, a steady-state assumption in Xe** within the laser pulse is valid,

$$[Xe^{**}]=\sigma^{(2)}[Xe]I^2/([N_2O]k_2+k_3). \quad (6)$$

As mentioned above, it is also necessary to take explicit account of the radiation intensity as it traverses the 1 cm path length of the solid, in the kinetic analysis. The coupled rate expressions that are numerically integrated are

$$\frac{d}{dt}[N_2O]=-[Xe^{**}][N_2O]k_2(\phi_{22}+\phi_{23}) +[O/Xe]I\sigma_1\phi_{43}+[O/N_2]I\sigma_2\phi_{53}, \quad (7)$$

$$\frac{d}{dt}[O/Xe]=[Xe^{**}][N_2O]k_2\phi_{23}+[O/N_2]I\sigma_2\phi_{52} -[O/Xe]I\sigma_1(\phi_{42}+\phi_{43}), \quad (8)$$

TABLE I. Kinetic parameters.

$\sigma^{(2)}(cm^4\ s)$	3.7×10^{-48}	(a) 3.7×10^{-48} (b) 2.4×10^{-49}
$k_2/k_3(cm^3)$	1×10^{-19}	
I(Å)	47	(c) 25–260
$\sigma_1(cm^2)$	8×10^{-19}	(d) 1×10^{-18}
$\sigma_2(cm^2)$	9.5×10^{-20}	
ϕ_{21}	0.15	
ϕ_{22}	0.00	
ϕ_{23}	0.85	
ϕ_{41}	0.365	
ϕ_{42}	0.43	
ϕ_{43}	0.205	
ϕ_{51}	0.08	
ϕ_{52}	0.71	
ϕ_{53}	0.21	

[a]Reference 1.
[b]Reference 9, p. 237.
[c]Reference 3.
[d]Estimated based on excitation spectrum and radiative lifetime of Xe^+O^- in Xe, from Ref. 4.

$$\frac{d}{dt}[O/N_2]=[Xe^{**}][N_2O]k_2\phi_{22}+[O/Xe]I\sigma_1\phi_{42} -[O/N_2]I\sigma_2(\phi_{52}+\phi_{53}), \quad (9)$$

$$-\frac{dI}{dt}=2\sigma^{(2)}[Xe]I^2+[O/Xe]I\sigma_1+[O/N_2]I\sigma_2. \quad (10)$$

The integration is carried out in both time and space. The latter is achieved by slicing the solid along the length of propagation of the radiation into optically thin segments, such that $\Delta I/I<0.01$ in each segment. The total N_2O concentration is summed over the entire length of the solid, to represent the concentrations that would be observed in the IR experiments. The instantaneous product of the radiation intensity and the O/Xe concentration in each segment is summed over all segments to represent the Xe^+O^- emission intensity measured in the fluorescence experiments.

The numerical solutions are then compared to the experiments, and the best fit parameters are obtained by iteration. We require the O atom concentration as a function of time to reproduce the photogeneration curves prior and subsequent to heat cycling, and the fractional N_2O loss at the end of the photogeneration to reproduce the IR measurement. Iteration of these solutions yields the set of rate constants and branching ratios collected in Table I. The time profiles simulated with these constants are shown together with the experimental data in Fig. 5.

The steady-state concentration of O/Xe as a function of pump intensity, shown in Fig. 4, represents an additional test of the model parameters. For the cyclic equilibrium, taking mass conservation into account, the equilibrium concentrations of the three species $[O/Xe]_e$, $[N_2O]_e$, $[O/N_2]_e$ can be related as

$$1/[O/Xe]_e$$

$$=1+[N_2O]_e/[O/Xe]_e+[O/N_2]_e/[O/Xe]_e, \quad (11a)$$

$$=1+\sigma_1\phi_{43}/\{I\sigma^{(2)}\phi_{23}[Xe]k_2/k_3\}+\sigma_1\phi_{42}/\sigma_2\phi_{52}. \quad (11b)$$

Therefore, a plot of $1/[O/Xe]_e$ vs $1/I$, should yield the equilibrium ratio of $[O/N_2]_e/[O/Xe]_e$ as its intercept, and the slope determines the equilibrium ratio of $[N_2O]_e/[O/Xe]_e$. Note however that Eq. (11) is valid for an optically thin sample. In the present case, it is necessary to consider the laser intensity profile, and the associated concentration profiles along the length of the solid. This is achieved by spatial integration of I,

$$I_z=I_0-\int\{I^2\sigma^{(2)}[Xe]+I\sigma_1[O/Xe]+I\sigma_2[O/N_2]\}dz. \quad (12)$$

Using Eq. (12), the equilibrium concentrations in optically thin slabs along the laser propagation are determined according to Eq. (11), and the observed steady-state signal is then related to $\int I_z[O/Xe]_z dz$, after normalization. Using the kinetic parameters of Table I, which were determined from the fits to time profiles, the dependence of the XeO steady-state emission on pump power is well reproduced, as illustrated in Fig. 4.

The simulations of photogeneration are carried out for a total irradiation of 3×10^{19} photons cm^{-2}. At the end of this period, 6% dissociation of N_2O is predicted. According to the IR spectra, the experiments show 8% dissociation. Given the scatter in the IR data, the agreement is deemed satisfactory.

In principle, there are ten independent variables in the simulated kinetics. These are the three absorption cross sections $\sigma^{(2)}$, σ_1, and σ_2, the volume spanned by the free exciton k_2/k_3, and two independent branching ratios in each of the processes of Eqs. (2), (4), and (5). These are determined by the following experimental observables: (a) The XeO growth profile at different laser intensities subject to two initial conditions. In the first photogeneration cycle $[N_2O]=[N_2O]_0$, $[O/Xe]=[O/N_2]=0$; and subsequent to heating $[N_2O]=[N_2O]_\infty$, $[O/Xe]=0$, $[O/N_2]=[O/Xe]_\infty$. (b) The XeO steady-state concentration as a function of pump intensity. (c) The N_2O time profiles as observed by the IR absorption measurements. The reproduction of all of these observables, with one set of kinetic parameters leads us to believe that, within the assumptions of the model, the parameters are well determined.

Independent checks exist for several of the determined parameters, and these are collected in Table I. The value derived from the simulations for the two-photon absorption cross section of Xe, $\sigma^{(2)}=3.7\times10^{-48}$ cm^4 s, is identical to that reported in Ref. 1. This exact agreement is fortuitous, since the measurements are subject to significant experimental error ($\sim$50% due to uncertainties associated with laser beam waist profile in the solid). From k_2/k_3 the diffusion range of free excitons in Xe, $l=(k_2/k_3)^{1/3}=47$ Å, is determined to be consistent with prior measurements, which range between 25–260 Å (see Table I). The absorption cross section of O/Xe, $\sigma_1=8\times10^{-19}$ cm^2, agrees with the estimate of this cross section based on its radiative lifetime and excitation profile. The absorption cross section of O/N_2 is mainly determined by the growth rates subsequent to heating the solid. A smaller value for this cross section than that of O/Xe is to be expected since O/N_2 corresponds to isolation of O atoms in sites that are significantly looser than interstitial traps.[4]

The dissociation limit of N_2O is determined by two effects (a) the reduction of the radiation field due to the O/Xe absorption, hence the reduced rate of two-photon absorption; (b) photoinduced regeneration of N_2O by the product oxygen atoms O/Xe and O/N_2. Note, although the absorption of O/N_2 is much smaller than that of O/Xe, its equilibrium concentration is much larger. At equilibrium, according to Eq. (11), $[O/N_2]_e/[O/Xe]_e=\sigma_1\phi_{42}/\sigma_2\phi_{52}=5.1$. Therefore, the main product of N_2O dissociation are photofragments trapped within the same cage.

The increased extent of dissociation at 266 nm is consistent with the above interpretation. The two photon excitation of the bulk xenon is expected to be similar for both 248 and 266 nm, but the oxygen atom photoproducts are not excited at 266 nm. Nevertheless, even after long periods of irradiation at 266 nm, according to the IR spectra, the N_2O dissociation is not complete. Using the same kinetic model, with the assumption of O atom absorption cross sections 100 times smaller, 13% dissociation of N_2O is predicted after deposition of 3×10^{19} photons cm^{-2} at 266 nm, as compared to the experimental value of 20%. Thus, although not studied in the same depth as the 248 nm data, the 266 nm data are consistently interpreted with the same kinetic model.

B. Mechanism

At the 8–10 eV of excitonic energy available to N_2O a variety of dissociative channels leading to $O(^1S, {}^1D)+N_2(^1\Sigma)$, $O(^3P)+N_2(^3\Sigma,{}^3\Pi)$, or $NO(^2\Pi)+N(^4S,{}^2D,{}^2P)$ are energetically possible.[10] Such dissociation products have previously been observed in vacuum ultraviolet (VUV) excited solid samples.[11] However, we see no direct evidence for any of these channels. We do not observe any detectable transient emissions from any atomic or molecular excited electronic states, and we have failed to see the formation of NO in the IR spectra. Although some of these dissociation channels would be difficult to eliminate without further experimental scrutiny, it is clear that the dissociation mechanism is not indiscriminate. This conclusion is reinforced by the absence of exciton mediated dissociation in O_2 doped solid Xe. Furthermore, the thermal recombination dynamics and photomobility induced steady-state dynamics observed in the present is quite different from that observed by 193 nm dissociation of N_2O in solid Xe, which proceeds via $N_2(^1\Sigma)+O(^1D)$ channel. As we have shown, the photodissociation of N_2O at 193 nm can be carried out to completion, and it has been shown that subsequent 248 nm irradiation of such solids leads to photodiffusion dominated by formation of O_2 instead of recombination.[6] The exciton induced dissociation of N_2O can therefore safely be ascribed to a specific channel,

namely, charge transfer induced dissociation which has its direct parallel in the gas phase.

It has been well established in gas phase studies that excited rare gas atoms, due to their reduced ionization energies, can be regarded as pseudo-alkalis, and as such can undergo harpoon reactions. More specifically, the harpoon reaction of N_2O with $Xe^*(6p)$ has been shown to be rather efficient,[12-15]

$$Xe^* + N_2O \rightarrow Xe^+N_2O^- \rightarrow N_2 + Xe^+O^-. \quad (13)$$

The same mechanism nicely explains the observed dynamics in the present. In contrast with the gas phase, where the ionic potentials are inaccessible for $Xe(6s)$,[14] due to solvation of ionic potentials, the energetic threshold for the entrance channel should be significantly lowered. This is consistent with the observation that two-photon excitation at 248 and 266 nm, which lead to the $n=2$, $J=1/2$ and $n=3$, $j=3/2$ excitons in Xe (Wannier notation),[3] are equally efficient in the photogeneration of O atoms. This mechanism, as in the gas phase, also explains the absence of O atom photogeneration in O_2 doped solids despite the fact that the $Xe^+O_2^-$ surface is energetically accessible. The nonreactivity in the case of O_2 is attributed to the stability of the O_2^- radical, in contrast with N_2O^- which is dissociative.[14]

The analogies with gas phase harpoon reactions and those in condensed media are strikingly similar. This has been borne out by our previous two-photon induced harpoon reactions with halogens in which intermolecular charge transfer states are accessed directly.[16] In general, in polarizable media, this ionic mechanism is observed to proceed with very large probabilities for cage exit of fragments. In fact, a "negative" cage effect has been postulated, i.e., one in which the cage atoms assist in the ejection of fragments.[16] The same is observed in the present. According to the kinetic analysis, the cage exit probability of O atoms in the present case is rather large, $\phi_{23}=0.85$. This process competes with recombination, and no in-cage dissociation is observed, $\phi_{22}=0$, although allowance is made for this channel in the kinetic analysis. An implication is that the cage exit does not proceed on the $O(^3P)$ surface, but rather on the ionic surface. The Xe^+O^- potentials are predissociative due to crossings with $O(^1D)$ and $O(^1S)$ surfaces. Thus, if such a surface hop occurs within the cage, recombination with N_2 should be expected. This presumably accounts for the recombination probability of $\phi_{21}=0.15$. Finally, dissociation via the ionic channel, assisted by the polarizable cage, would imply that the photoproducts are isolated as nearest neighbors. This would explain the effective thermal and photo-induced cage re-entry of O atoms. In contrast, the photo-induced recombination of O atoms generated by 193 nm irradiation is more consistent with photofragments that are separated by several lattice sites.[6,17] This is consistent with the $N_2+O(^1D)$ channel, and the expectation of facile mobility for $O(^1D)$, which is argued below.

Independent of the details of the dissociation channels, it is clear that photoexcitation of O atoms leads to facile crossing of cage barriers—O atoms are photomobile. We

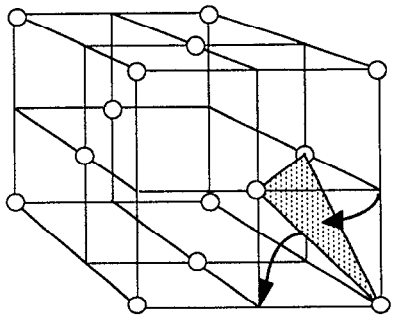

FIG. 6. The minimum energy path for an octahedral interstitial impurity migration is via the D_{3h} window shown as the shaded triangle in the fcc lattice. Note the same window is crossed for cage exit of photodissociation fragments from a substitutionally trapped parent.

observe cage reentry with ~20% probability of recombination with N_2 ($\phi_{43}=0.205$). This channel is only consistent for migration of electronically excited O atoms. The observed formation of O/N_2 by photomobility of O atoms is not in contradiction with this expectation. Broadside collision of excited atoms with N_2 could lead to quenching to form $O(^3P)$ trapped next to N_2. However, the observations that the generation of Xe^+O^- within the cage containing N_2 does not yield O/N_2 with any significant probability ($\phi_{51}=0.08$ and $\phi_{22}=0$) would argue that the observed cage re-entry of photo-mobilized atoms mainly proceeds via the $O(^1D)$ surface.

Extensive photomobility of ground state F atoms has been documented previously both by experiment[18] and theory.[19] In effect F atoms are "small," as judged by F–Rg pair potentials. In fact, based on diatomic potential parameters, potential minimum and repulsive wall, of all known ground state atoms, F has the shortest interaction range with rare gases. The diatomic pair potentials of Xe–O have been calculated,[20] and the ground state potential has been extracted from molecular beam scattering data.[21] These have been recently shown to be at least qualitatively consistent with the observed spectroscopy in solid Xe.[4] The interaction is quite repulsive in the ground ^3P state, and it is clear that trapping in this state is stable. In contrast, $O(^1D)$ forms a bound potential $^1\Sigma^+$ with an internuclear separation of 2.2 Å,[4] more than 1 Å shorter than in the ground state minimum, which occurs near 3.7 Å. In this excited state, the O atom has shrunk to a size comparable to F.

Consideration of the dividing surfaces that must be crossed for atomic mobility from one lattice site to another, for different electronic configurations, is quite illuminating. Exact multidimensional surfaces are not available. However, relying on the spectroscopic information available, schematic surfaces, correlation diagrams, can be constructed. Consider a fcc solid with an O atom trapped at the interstitial octahedral site, which is believed to be the probed population. The minimum energy path to cross to a new equivalent site requires passage through the D_{3h} window, via a curved path, as indicated in Fig. 6. The internuclear distance between an impurity atom trapped in this

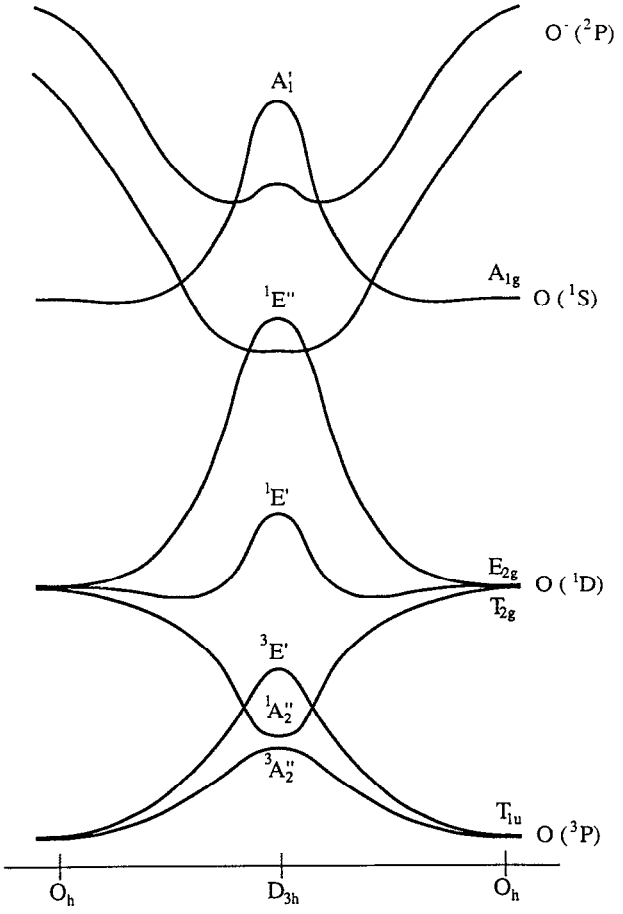

FIG. 7. A schematic of the potential energy surface cuts along the coordinate of Fig. 6, for O atoms in solid Xe. The potentials are based on the spectroscopic analysis in Ref. 4.

undistorted window, and the rare gas atoms is given as $r(D_{3h})=(6^{1/2}/6)d=2.5$ Å in Xe ($d=6.13$ Å=lattice constant of Xe). At this interaction range, the ^3P surface is highly repulsive, ~0.5 eV/Xe atom. However, for the case of the $1\,^1\Sigma^+$ state, the window is larger than the diatomic potential minimum. We would therefore expect the summation over three nearest-neighbor Xe atoms to further increase this binding, and indeed the solid state potential minimum in this state is observed to be twice that of the theoretical diatomic potential.[4] A schematic for the variety of surfaces that arise from excited and ground O atom interactions with Xe along the cage exit coordinate, O_h–D_{3h}–O_h, is shown in Fig. 7. In the case of the charge transfer potentials, we do not believe the surfaces to be additive over nearest neighbors, since it was shown that the binding derives its main character from the diatomic Xe^+O^- configuration, which is isoelectronic with the *I*Cl, and therefore due to specific overlap with a single nearest neighbor. Nevertheless, the charge transfer state also shows a soft minimum at an internuclear separation of 2.32 Å, therefore at the D_{3h} geometry. In fact, structured emission is observed between the diatomic $3\,^1\Sigma^+ \rightarrow 1\,^1\Sigma^+$ potentials, which correspond to the bound–bound, $^1E'' \rightarrow {}^1A_2''$ transition in the D_{3h} window.[4] The present surfaces therefore provide a better rationalization as to the origin of recursions on this surface. Essentially, in the window, the $O(^1D)$ atoms are bound along all directions and may only relax by curve crossing to the triplet surface. Similar dynamics should prevail in the ionic surface. Since O^- fits well in the cage windows, it will experience a potential minimum there. Curve crossing to neutral potentials can therefore carry the atom to the octahedral sites.

V. CONCLUSIONS

In highly diluted rare gas solids, UV laser irradiation can lead to multiphoton access of excitonic states, and exciton-induced dissociation of impurities becomes an important photodissociation mechanism for impurities in which the negative ion is unbound. Exciton induced dissociation of molecular impurities by direct optical access of rare gas excitons has previously been observed. Of particular relevance to the present are the studies on N_2O, CO_2, and O_2 doped krypton and Xe matrices.[22–24] The harpooning mechanism had been invoked in the interpretation of the data.[23] In the case of N_2O doped Xe solids, specific production of $O(^1D)$ is concluded. However we have reassigned the emission used in this interpretation to Xe^+O^-,[4] and therefore the exciton induced reactions should be reassigned to the ionic channel. It should also be pointed out that these VUV studies do not distinguish between emissions due to permanent dissociation vs transient species which may undergo in-cage recombination. The kinetic analysis in the present provides a rather clear picture of the dominant dynamics of permanent reactions.

Extensive photomobility of O atoms via access of charge transfer potentials is observed, and rationalized by the topology of excited electronic surfaces. While exact surfaces do not yet exist, schematic correlations along the cage exit coordinate reveal that although a cage barrier exists in the ground state of O atoms, in both $O(^1D)$ and O^-, minima develop at the dividing surface between trapping sites. It can be therefore predicted that extensive long-range mobility of O atoms should be observed on the ^1D state, and site-to-site hopping should be observed on the ionic surface. The distinction between these two is based on the nature of the potentials; while additivity is present in the neutral potentials, the ionic potentials in this case are believed to be highly localized.

It should be clear that the photochemistry observed in these systems is strongly controlled by nonadiabatic dynamics. As such a deeper understanding of the many-body electronic surfaces, and their couplings is essential for detailed analyses. There is a need for theoretical treatments of multisurface dynamics in these model systems.

ACKNOWLEDGMENTS

This research was supported by the U.S. Air Force Phillips Laboratory under Contract No. S04611-90-K-0035, and by a grant from the National Science Foundation, ECS-8914321. The 266 nm experiments, and the IR studies were conducted in the Laser Spectroscopy Facility

of the Department of Chemistry at UCI. Useful discussions with Professor N. Schwentner and D. Imre, are gratefully acknowledged.

[1] T. Kessler, R. Markus, H. Nahme, and N. Schwenter, Phys. Status Solidi B **139**, 619 (1987).
[2] E. H. Böttcher and W. F. Schmidt, Phys. Status Solidi B **126**, K 165 (1984).
[3] N. Schwentner, E. E. Koch, and J. Jortner, *Electronic Excitations in Condensed Rare Gases*, Springer Tracts in Modern Physics (Springer, New York, 1985), Vol. 107.
[4] W. G. Lawrence and V. A. Apkarian, J. Chem. Phys. **97**, 2229 (1992).
[5] W. G. Lawrence and V. A. Apkarian, J. Chem. Phys. **97**, 2224 (1992).
[6] H. Kreuger and E. Weitz, J. Chem. Phys. **96**, 2846 (1992).
[7] C. Hubrich and F. Stuhl, J. Photochem. **12**, 93 (1980).
[8] M. F. Merienne, B. Coquart, and A. Jenouvrier, Planet. Space. Sci. **38**, 617 (1990).
[9] K. Hohla, H. Pummer, and C. K. Rhodes, *Excimer Lasers*, edited by C. K. Rhodes (Springer, New York, 1984), Chap. 8.
[10] (a) A. Chutjian and G. A. Segal, J. Chem. Phys. **57**, 3069 (1972); (b) D. G. Hopper, *ibid.* **80**, 4290 (1984).
[11] J. M. Brom and H. P. Broida, Chem. Phys. Lett. **33**, 384 (1975).
[12] J. E. Velazco and D. W. Setser, Chem. Phys. Lett. **25**, 197 (1974).
[13] J. E. Velazco, J. H. Kolts, and D. W. Setser, J. Chem. Phys. **69**, 4357 (1978).
[14] J. Xu, D. W. Setser, and J. K. Ku, Chem. Phys. Lett. **132**, 427 (1986).
[15] A. Kvaran, A. Ludviksson, W. S. Hartree, and J. P. Simons, Chem. Phys. Lett. **137**, 209 (1987).
[16] M. E. Fajardo and V. A. Apkarian, J. Chem. Phys. **89**, 4102 (1988).
[17] E. Weitz (private communications).
[18] J. Feld, H. Kunttu, and V. A. Apkarian, J. Chem. Phys. **93**, 1009 (1990); H. Kunttu, J. Feld, R. Alimi, and V. A. Apkarian, *ibid.* **92**, 4856 (1990).
[19] R. Alimi, R. B. Gerber, and V. A. Apkarian, J. Chem. Phys. **92**, 3551 (1990).
[20] T. H. Dunning and P. J. Hay, J. Chem. Phys. **66**, 3767 (1977).
[21] V. Aquilanti, R. Candori, and F. Pirani, J. Chem. Phys. **89**, 6157 (1988).
[22] K. M. Monahan and V. Rehn, J. Chem. Phys. **68**, 3814 (1978).
[23] R. V. Taylor, W. Scott, P. R. Findley, Zenglie Wu, and W. C. Monahan, J. Chem. Phys. **74**, 3718 (1981).
[24] R. V. Taylor and W. C. Walker, J. Chem. Phys. **70**, 284 (1979).